



Geophysical Research Letters[®]

RESEARCH LETTER

10.1029/2022GL098064

Key Points:

- The large Antarctic ozone holes of 2020 and 2021 were accompanied by stratospheric burdens of wildfire and volcanic emissions, respectively
- Both ozone holes were associated with pronounced changes in surface climate consistent with the impacts of Antarctic ozone depletion
- Together, the linkages suggest that both wildfire smoke and volcanic emissions can lead to large-scale changes in surface climate

Supporting Information:

Supporting Information may be found in the online version of this article.

Correspondence to:

S. Yook,
simchan.yook@colostate.edu

Citation:

Yook, S., Thompson, D. W. J., & Solomon, S. (2022). Climate impacts and potential drivers of the unprecedented Antarctic ozone holes of 2020 and 2021. *Geophysical Research Letters*, 49, e2022GL098064. <https://doi.org/10.1029/2022GL098064>

Received 25 JAN 2022

Accepted 11 MAY 2022

Author Contributions:

Conceptualization: Simchan Yook, David W. J. Thompson, Susan Solomon
Data curation: Simchan Yook
Formal analysis: Simchan Yook
Funding acquisition: David W. J. Thompson, Susan Solomon
Supervision: David W. J. Thompson, Susan Solomon
Writing – original draft: Simchan Yook, David W. J. Thompson, Susan Solomon
Writing – review & editing: Simchan Yook, David W. J. Thompson, Susan Solomon

© 2022. The Authors.

This is an open access article under the terms of the [Creative Commons Attribution License](#), which permits use, distribution and reproduction in any medium, provided the original work is properly cited.

Climate Impacts and Potential Drivers of the Unprecedented Antarctic Ozone Holes of 2020 and 2021

Simchan Yook¹ , David W. J. Thompson^{1,2} , and Susan Solomon³ 

¹Department of Atmospheric Science, Colorado State University, Fort Collins, CO, USA, ²School of Environmental Sciences, University of East Anglia, Norwich, UK, ³Department of Earth, Atmospheric, and Planetary Sciences, Massachusetts Institute of Technology, Cambridge, MA, USA

Abstract The latter months of 2020 and 2021 were marked by two of the largest Antarctic ozone holes on record. That such large ozone holes occurred despite ongoing ozone recovery raises questions about their origins and climate impacts. Here we provide novel evidence that supports the hypothesis that the ozone holes were influenced by two distinct and extraordinary events: the Australian wildfires of early 2020 and the eruption of La Soufrière in 2021. We further reveal that both ozone holes were associated with widespread changes in Southern Hemisphere climate that are consistent with the established climate impacts of Antarctic ozone depletion, including a strengthening of the polar stratospheric vortex, enhanced surface westerlies over the Southern Ocean, and surface temperature changes over Antarctica and Australia. The results thus provide suggestive evidence that injections of both wildfire smoke and volcanic emissions into the stratosphere can lead to hemispheric-scale changes in surface climate.

Plain Language Summary The Antarctic ozone hole is characterized by dramatic decreases in stratospheric ozone during the austral spring months. The ozone hole is expected to recover over the next few decades in response to the phasing out of ozone-depleting substances. However, the latter months of 2020 and 2021 were marked by two of the largest Antarctic ozone holes on record, which raises questions about their origins and climate impacts. Here we provide novel evidence that supports the hypothesis that the ozone holes were influenced by two extraordinary events: the Australian wildfires of early 2020 and the eruption of La Soufrière in 2021. We further reveal that both ozone holes were associated with changes in Southern Hemisphere surface climate consistent with the established climate impacts of Antarctic ozone depletion. Together, the results provide suggestive evidence that injections of both wildfire smoke and volcanic emissions into the stratosphere can lead to hemispheric-scale changes in surface climate.

1. Introduction

The Antarctic ozone hole has a pronounced effect on Southern Hemisphere surface climate (Fogt & Marshall, 2020; Polvani et al., 2011; Thompson et al., 2011; Thompson & Solomon, 2002). The radiative effects of polar ozone depletion act to cool and strengthen the stratospheric polar vortex (Randel & Wu, 1999; Waugh et al., 1999), and dynamical coupling between the stratosphere and troposphere acts to connect the changes in the stratospheric flow to the surface (Baldwin & Dunkerton, 2001; Thompson et al., 2005). At the surface, the changes in the flow associated with the ozone hole project onto the southern annular mode (Shindell & Schmidt, 2004; Thompson & Solomon, 2002). Thus the ozone hole has been linked to long-term changes in surface climate that span much of the Southern Hemisphere mid and high latitudes.

The linkages between the Antarctic ozone hole and the SAM are important for the interpretation of Southern Hemisphere climate change. Over the 1970–1990s, the development of the ozone hole was associated with widespread changes in Southern Hemisphere surface climate that are consistent with forcing by ozone depletion (Thompson et al., 2011). Paleoclimate studies indicate that the resulting changes in the austral summer SAM index are unprecedented over the last thousand years, pointing toward the remarkable role of the ozone hole in Southern Hemisphere climate change (Fogt & Marshall, 2020).

In recent years, the Antarctic ozone hole has exhibited signs of healing consistent with recent decreases in anthropogenic emissions of ozone-depleting substances (Solomon et al., 2016). The healing of the ozone hole is apparent when viewed in the context of decades, especially during September when dynamic variability in the vortex is modest (Abrahamsen et al., 2020; Hassler et al., 2011; Solomon et al., 2016; Strahan et al., 2019). Recent studies

have correspondingly shown that trends in the SAM have paused or slightly reversed (Banerjee et al., 2020; Zambri et al., 2021). Yet the ozone holes of late 2020 and 2021 rate amongst some of the largest on record during October and later months, and they have obscured the overall trend toward recovery of the ozone hole (<https://ozonewatch.gsfc.nasa.gov>; Stone et al., 2021).

Why were the ozone holes of 2020 and 2021 so large given the overall trend toward ozone recovery? One possibility is internal dynamical variability. That is: the ozone hole forms due to chemical processes, but atmospheric dynamics contribute to year-to-year variations in its size and strength, particularly during October and November (Randel et al., 2002; Safieddine et al., 2020; Shindell et al., 1997; Wargan et al., 2020; Weber et al., 2011). Years marked by anomalously weak extratropical stratospheric wave driving are associated with anomalously low polar cap ozone concentrations due to both (a) dynamically induced changes in ozone transport and (b) feedbacks between polar stratospheric temperatures and heterogeneous ozone chemistry. The Southern Hemisphere stratospheric wave driving was unusually weak in late 2020 and 2021 (<https://ozonewatch.gsfc.nasa.gov>) and thus dynamical processes likely contributed to the size of the 2020 and 2021 ozone holes.

Another possibility is that the 2020 and 2021 ozone holes were influenced by anomalously large stratospheric aerosol loadings due to two episodic events: The catastrophic Australian bushfires of early 2020 and the April 2021 eruption of La Soufrière on Saint Vincent.

The Australian bushfires of early 2020 injected large amounts of particulate matter into the stratosphere (Ansmann et al., 2022; Hirsch & Koren, 2021; Khaykin et al., 2020; Magaritz-Ronen & Raveh-Rubin, 2021; Ohneiser et al., 2020; Peterson et al., 2021; Schwartz et al., 2020; Yu et al., 2021). Observations indicate that some of the smoke settled into the Southern Hemisphere polar stratosphere in the latter part of 2020 (Ansmann et al., 2022; Khaykin et al., 2020; Peterson et al., 2021; Yu et al., 2021). Wildfire smoke is theorized to contribute to ozone depletion if the smoke particles become coated with sulfuric acid and water as they age, so that they behave like liquid polar stratospheric cloud particles and thus provide a surface for heterogeneous chemistry (Ansmann et al., 2021, 2022; Yu et al., 2021). Solomon et al. (2022) provide observational evidence supporting this view.

The April 2021 eruption of La Soufrière on Saint Vincent contributed to the stratospheric sulfate aerosol burden in the tropics in mid-2021 (Babu et al., 2021) and—as suggested here—late-2021 as well. Previous work has argued that volcanic eruptions can influence the stratospheric circulation through a variety of processes. The absorption of longwave radiation by volcanic aerosols directly influences stratospheric temperatures and thus winds (e.g., DallaSanta et al., 2019; Kodera, 1994; Robock, 2000; Robock & Mao, 1995; Toohey et al., 2014); indirect mechanisms have also been proposed (e.g., Coupe & Robock, 2021). The resulting changes in stratospheric temperatures and winds can contribute to changes in ozone transport and temperature-dependent heterogeneous ozone chemistry (Langematz et al., 2018; Weber et al., 2011). And volcanic sulfuric acid aerosols provide a surface for heterogeneous ozone chemistry (Portmann et al., 1996; Solomon, 1999; Solomon et al., 2016; Tabazadeh et al., 2002; Wilka et al., 2018).

Here we demonstrate that both the 2020 and 2021 Antarctic ozone holes were associated not only with large stratospheric aerosol loadings but also pronounced changes in the Southern Hemisphere circulation that extended from the stratosphere to the surface. Our goal is not to prove the specific physical mechanisms that drove the unusual 2020 and 2021 Antarctic ozone holes. Rather, it is to document a series of physically consistent linkages between the Australian bush fires in early 2020, the eruption of La Soufrière on Saint Vincent in April 2021, the 2020 and 2021 ozone holes, and hemispheric-scale changes in the Southern Hemisphere tropospheric circulation. The results are of interest irrespective of causal factors. If the 2020 and 2021 ozone holes arose due to internal variability or dynamical forcing by particulate matter, then the results point to surprising effects of the ozone hole on SH surface climate despite evidence for ozone recovery. If the unusually strong 2021 ozone hole was influenced by the eruption of La Soufrière, then the results add to the already substantial body of evidence that volcanoes influence surface climate over regions far removed from the eruption itself. And if the unusually strong 2020 ozone hole was influenced by smoke from the Australian bush fires, then the results suggest that large injections of wildfire smoke into the stratosphere can lead to widespread changes in surface climate that persist long after the cessation of smoke production.

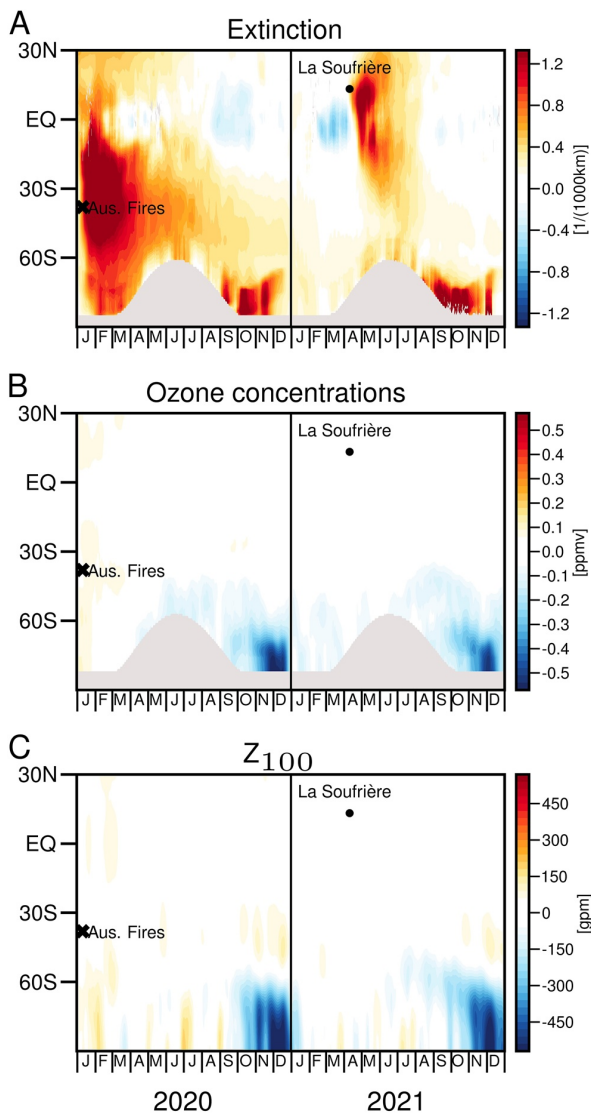


Figure 1. Time series of zonal-mean stratospheric aerosol extinction, ozone concentrations, and geopotential height anomalies during 2020–2021. Results are shown at the 100 hPa level (Panels (a) and (b)) are shown at the 70 hPa level in Figure S1. The cross and dot indicate the Australian bushfires of early 2020 and the April 2021 eruption of La Soufrière, respectively. Aerosol extinction (A, 10^{-3} km^{-1}) and ozone concentrations (B, ppmv) are derived from the Ozone Mapping and Profiler Suite Limb Profiler instrument. Geopotential heights (C, in geopotential meters; gpm) are derived from ERA5. Anomalies are calculated with respect to the base period 2012–2019 (omitting 2015 due to the eruption of Calbuco). The results are smoothed with an 11-point (11-degree by 11-day) running mean filter.

2. Data and Methods

Ozone and extinction values for 2020 and 2021 are based on data from the Ozone Mapping and Profiler Suite Limb Profiler (OMPS-LP) instrument (Taha et al., 2021; Zawada et al., 2018). OMPS-LP measurements have been used in numerous studies of the Antarctic ozone hole (Kramarova et al., 2014; Rieger et al., 2021; Yu et al., 2021). Aerosol extinction is retrieved at a single wavelength channel of 745 nm and clouds are removed using the cloud detection algorithm (Chen et al., 2016). OMPS-LP ozone concentrations below 10 hPa are derived from visible wavelengths. OMPS-LP observations are weighted for the number of samples when observations are available, and area averages are weighted by pressure and the cosine of latitude as necessary. Tropospheric aerosol extinction and ozone concentrations are neglected in the calculations of all vertical averages.

Ozone values for the extended 1979–2021 period were obtained from the NASA ozone watch and consist of Southern Hemisphere polar cap ozone hole area and total column ozone values (<http://ozonewatch.gsfc.nasa.gov>). Atmospheric temperatures, winds, and geopotential height are based on the European Center for Medium-Range Weather Forecasts Re-Analysis 5 (ERA5; Hersbach et al., 2020).

All results are shown as anomalies with respect to the 2012–2019 mean seasonal cycle (the OMPS-LP data are available starting 2012). We omit 2015 from the base climatology since it was marked by large stratospheric aerosol loadings from the Calbuco eruption (Zhu et al., 2018).

3. Results and Discussion

3.1. Aerosol Burdens and Ozone Depletion in 2020 and 2021

Figures 1 and 2a summarize the aerosol loadings that occurred in the Southern Hemisphere over the 2020–2021 period. Figure 1a shows extinction at 100 hPa as a function of latitude and day of year; Figure 2a shows extinction averaged over the extratropics (30–90S) as a function of height and day. As shown in previous studies (Ansmann et al., 2022; Khaykin et al., 2020; Peterson et al., 2021; Yu et al., 2021), the SH lower stratosphere was marked by enhanced extinction values throughout 2020. Extinction increased rapidly following the Australian bush fires in January and persisted throughout the SH middle and high latitudes until at least the end of the year (Figures 1a and 2a; Ansmann et al., 2022; Khaykin et al., 2020; Peterson et al., 2021; Yu et al., 2021). The lag between the fires in early 2020 and the emergence of high extinction values in the lower polar stratosphere in late 2020 (Figure 1a) is consistent with the lofting of material at low latitudes followed by the poleward transport and descent of particles at polar latitudes (see also Rieger et al., 2021, Figure 3). The signature of the fires is partially obscured by the lack of data in polar night (Figure 1a) and below the tropopause (Figure 2a). Nevertheless, the time evolution of extinction in 2020 strongly suggests that the high polar values found in late 2020 originated from the Australian fires that occurred earlier that year (Yu et al., 2021).

The SH lower stratosphere was also marked by enhanced extinction values throughout 2021. In this case, the increases in extinction began soon after the eruption of La Soufrière in the tropics (Figures 1a and 2a). Interestingly, the polar extinction anomalies in late 2021 are comparable to those in late 2020. It is noteworthy that the extinction values are shown with respect to the OMPS climatology in years without major eruptions (Methods), and thus the high values at polar latitudes do

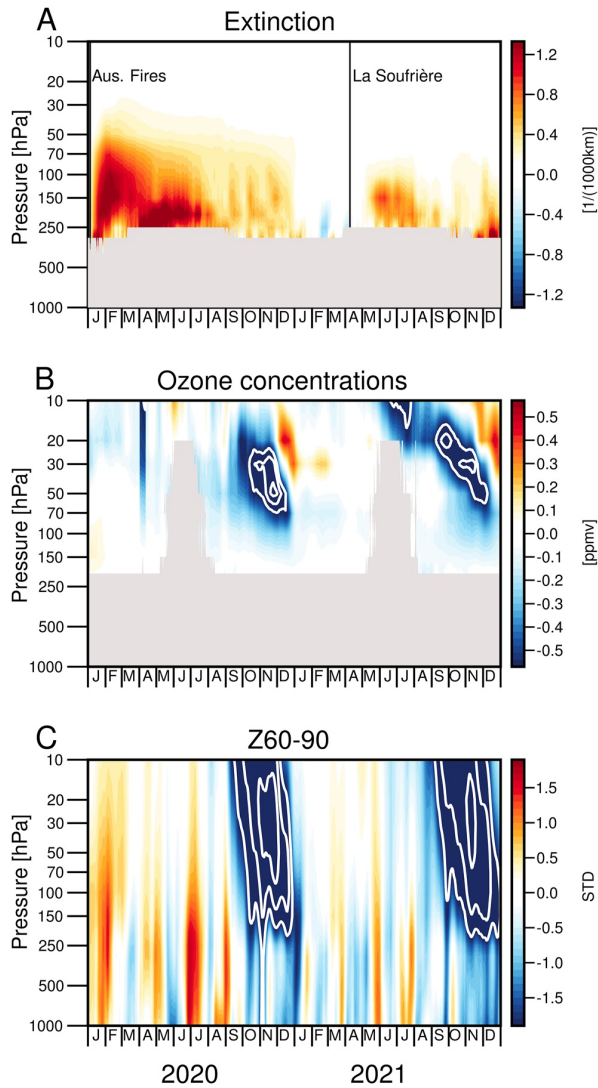


Figure 2. Time series of area-mean stratospheric aerosol extinction, ozone concentrations, and polar cap geopotential height anomalies. Ozone Mapping and Profiler Suite Limb Profiler aerosol extinction data (A, 10^{-3} km^{-1}) are averaged over $30\text{--}90^\circ$, ozone concentrations (B, ppmv) are averaged over $50\text{--}90^\circ$, and geopotential anomalies (C, normalized) are averaged over $60\text{--}90^\circ$. White contour lines are spaced at $-0.6, -0.8, -1.0\ldots$ ppmv for the ozone anomalies and $\pm 2, 3, 4\ldots$ gpm for the geopotential anomalies. Black lines in the top panel mark the onset day of the Australian bushfires and the La Soufrière eruption. Regions within the troposphere or with a relatively small number (<200) of observations are masked out. The results are smoothed with an 11-day running mean filter. Anomalies are calculated with respect to the base period 2012–2019 (omitting 2015 due to the eruption of Calbuco).

scatter plots highlight both (a) the robust nature of the linkages between the ozone hole and the SH circulation and (b) the extraordinary nature of the 2020 and 2021 spring seasons. Note that the results in the left panel are shown for the OMPS period of record only while results in the middle and right panels are shown for the period starting 1979 (Methods).

not reflect the seasonal cycle of aerosol loadings. Further, the OMPS aerosol extinction values are based on a cloud screened version of the data which filters out the possible influence of clouds, including polar stratospheric clouds (Chen et al., 2016).

Figures 1 and 2b summarize the attendant anomalies in ozone concentration. Figure 1b again shows results at 100 hPa while Figure 2b shows results averaged over the polar regions (50–90S). The ozone anomalies are shown with respect to the same base as that period used for extinction. As noted in Stone et al. (2021), the 2020 ozone hole was among the largest on record in October. From Figures 1 and 2b, it is clear that the 2021 polar ozone anomalies were comparable in magnitude to those found in 2020. Interestingly, the large 2021 ozone hole was preceded by large wintertime ozone anomalies in the middle stratosphere that bear the hallmark of dynamic variability (Figure 2b). The unusual nature of the 2020 and 2021 ozone holes is apparent in their sizes (Stone et al., 2021). It is also apparent in the magnitude of the ozone anomalies with respect to the rest of the OMPS record (Figures 1b and 2b).

3.2. Connections to the Hemispheric-Scale Circulation and Surface Climate

Figures 1 and 2c summarize the accompanying changes in the atmospheric circulation. Figure 1c shows the changes in geopotential height at 100 hPa; Figure 2c reveals the vertical structure of geopotential height anomalies averaged over the polar cap (60–90S). The 2020 and 2021 ozone holes were both associated with large decreases in polar stratospheric geopotential consistent with cooling of the polar cap (Figure 1c). The decreases in polar geopotential height reflect a strengthening of the circumpolar vortex and thus positive anomalies in the southern annular mode at stratospheric levels. Consistent with our understanding of stratosphere/troposphere coupling (Baldwin & Dunkerton, 2001; Fogt & Marshall, 2020; Kidston et al., 2015; Thompson et al., 2005), the anomalies in the stratospheric circumpolar flow extend to Earth's surface over a period of several weeks during both late 2020 and late 2021 (Figure 2c).

The extension of the circulation anomalies to tropospheric levels is clearly reflected in various changes in surface climate during late 2020 and 2021. Tropospheric geopotential height exhibited anomalies that resemble the high index polarity of the southern annular mode at tropospheric levels during both the 2020 and 2021 late austral spring/early summer seasons (Figures 3a and 3b). The attendant changes in the surface circulation include various established regional climate impacts of the SAM, including anomalously westerlies over much of the Southern Ocean (Figures 3c and 3d), anomalously cool conditions over the Antarctic plateau juxtaposed against warm conditions over the Antarctic peninsula (Figures 3c and 3d; Thompson & Solomon, 2002), and anomalously cool conditions over much of Australia (Figures 4e and 4f; Hendon et al., 2007).

Figure 4 shows SH polar ozone anomalies plotted against SH extratropical-mean extinction (Figure 4a), the SH large-scale stratospheric circulation (Figure 4b), and the SH large-scale tropospheric circulation (Figure 4c). The

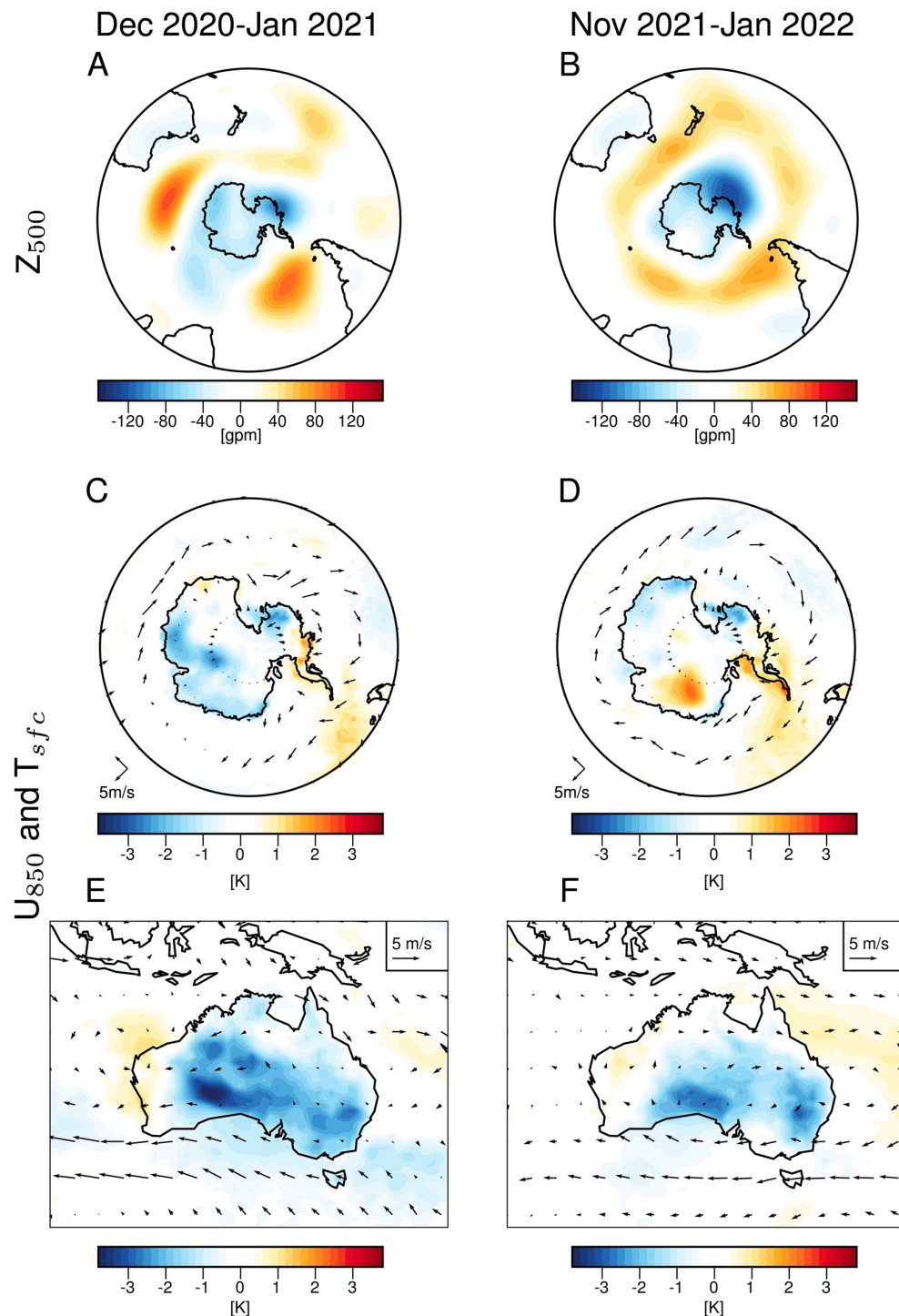


Figure 3. Surface climate anomalies during the 2020 and 2021 seasons. Monthly mean anomalies in (a, b) geopotential height at 500 hPa (gpm) in the SH (c–f) 2m-air temperature and the 850 hPa flow over (c, d) the Antarctic and (e, f) Australia. Results are shown for the periods of (a, c, e) December–January in 2020/21 and (b, d, f) November–January in 2021/22. Anomalies are calculated with respect to the base period 2012–2019 (omitting 2015 due to the eruption of Calbuco).

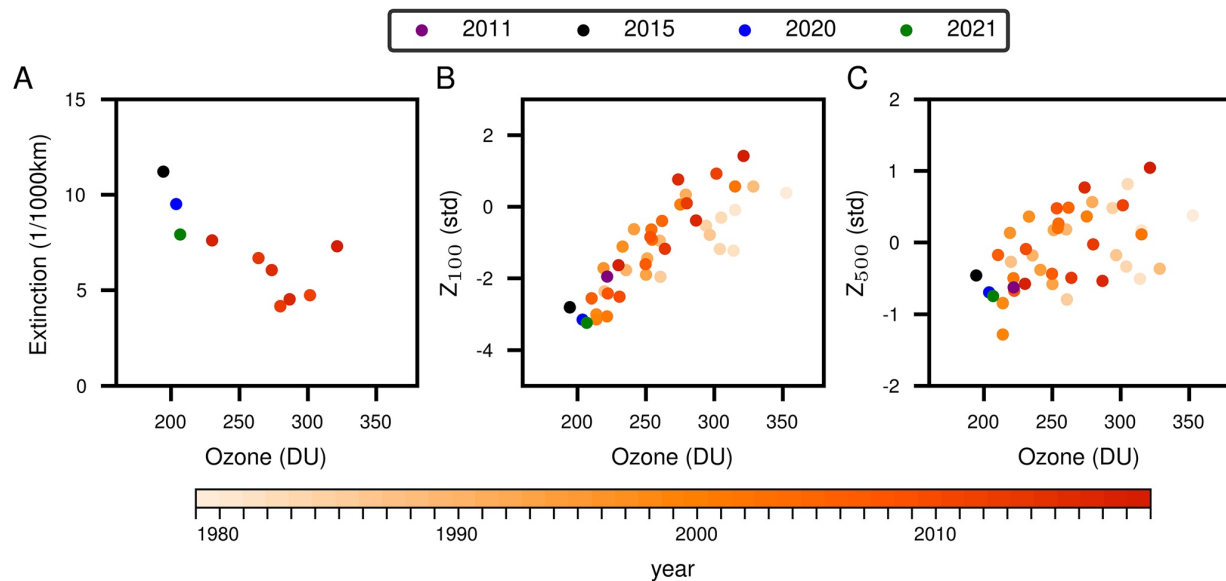


Figure 4. Scatter plots of total column ozone derived from the NASA Ozone Watch averaged over October to November (abscissa) versus (a) Ozone Mapping and Profiler Suite total column stratospheric aerosol extinction averaged over October to November, ERA5 polar cap geopotential height at (b) 100 hPa averaged over November to December and (C) 500 hPa averaged over November to January. The aerosol extinction data are averaged 30° – 90° ; ozone concentrations are averaged 63° – 90° ; and geopotential heights are averaged 60° – 90° . Selected years with high aerosol loadings are indicated by the top colorbar; other years are indicated by the bottom colorbar. Anomalies are calculated with respect to the base period 2012–2019 (omitting 2015 due to the eruption of Calbuco).

The extinction anomalies during October–November of 2020 and 2021 (Figure 4a; blue and green dots) were exceeded only by those found after the eruption of the Calbuco volcano in 2015 (black dot). All 3 years were associated with extreme column ozone losses (left) and, in turn, anomalously low polar stratospheric geopotential heights (middle). The outlier in Figure 4a, when ozone reached \sim 325DU but extinction was not extremely low, was associated with the minor sudden stratospheric warming event in 2019 and is thus consistent with dynamic variability (Safieddine et al., 2020; Shen et al., 2020; Wagan et al., 2020). Other years marked by low polar ozone and stratospheric geopotential height anomalies include 2011, which coincides with the eruption of Cordon Caulle (purple dot in the middle panel), and the late 1990s, which coincide with the period of largest stratospheric chlorine loadings (dark orange dots). Apparently, extreme ozone losses and stratospheric geopotential height falls are associated with large chlorine loadings and/or enhanced particulate matter.

The years 2011, 2015, 2020 and 2021 also standout in terms of the attendant anomalies in the tropospheric circulation (right panel). All 4 years are associated with relatively low values of polar geopotential height at tropospheric levels during the late spring months indicative of the positive index polarity of the SAM.

Taken together, the scatter plots in Figure 4 reveal that both 2020 and 2021 stand out in terms of extinction (left ordinate), column ozone losses (abscissas), changes in the stratospheric circulation (middle ordinate), and changes in the tropospheric circulation (right ordinate). Note that the fits in all three panels are highly significant ($p < 0.01$) based on the t-statistic assuming one degree of freedom per calendar year, and that the associated variances explained by the linear fits are extremely high (\sim 60%, 70% and 26% for panels a–c, respectively). The results are not sensitive to the latitudinal domain used to average the aerosol extinction values, that is, similar results are derived using domains spanning 30° – 90° S to 60° – 90° S.

The uniqueness of the 2020 and 2021 seasons is further highlighted by the histograms in Figure 5. The gray bars indicate histograms of daily values for all years in the record (Methods); the colored bars indicate histograms of daily values during late 2020 (left) and 2021 (right). The histograms are normalized such that the largest value on the ordinate axis is the same for 2020, 2021, and the historical periods; the number of days used to populate each histogram is indicated on the figures. Again, it is clear that both late 2020 and 2021 were marked by unusually high values of extinction (top), low concentrations of polar ozone (second from top), and low pressures in the

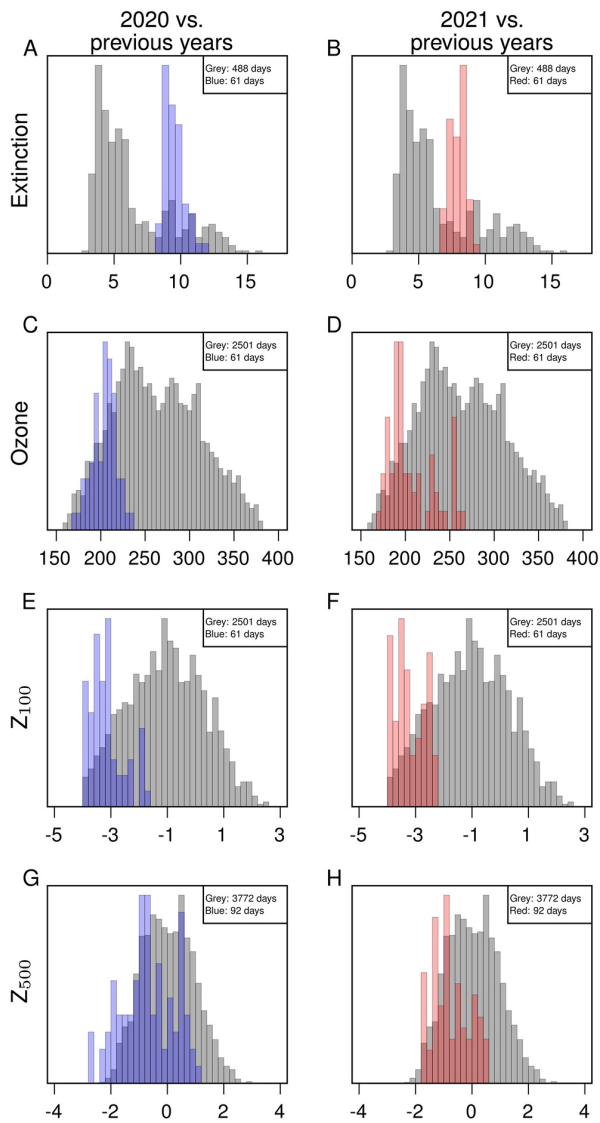


Figure 5. Histograms of daily mean, Ozone Mapping and Profiler Suite total column stratospheric aerosol extinction, NASA Ozone Watch total column ozone, and ERA5 geopotential height anomalies at indicated levels. Results are derived from all days during October–November for aerosol extinction and total column ozone, November–December for 100 hPa height, November–January for 500 hPa height. The aerosol extinction data are averaged 30°–90°; ozone concentrations are averaged 63°–90°; and geopotential heights are averaged 60°–90°. Colored bars denote days during 2020 and 2021; gray bars denote days during all other years in the available record. The PDFs are normalized to the same height; the number of days used to construct the PDFs is indicated on the plots. Anomalies are calculated with respect to the base period 2012–2019 (omitting 2015 due to the eruption of Calbuco).

OMPS-LP aerosol and ozone data are available at the Goddard Disc (https://disc.gsfc.nasa.gov/datasets/OMPS_NPP_LP_L2_AER_DAILY_2/summary?keywords=OMPS_NPP_LP_L2_AER_DAILY_2 and [https://disc.gsfc.nasa.gov/datasets/OMPS_NPP_LP_L2_O3_DAILY_2](https://disc.gsfc.nasa.gov/datasets/OMPS_NPP_LP_L2_O3_DAILY_2/summary?keywords=OMPS_NPP_LP_L2_O3_DAILY_2)), polar cap ozone data are

polar atmosphere consistent with a strengthening of the circumpolar westerly from the stratospheric levels to the surface (bottom two rows).

4. Conclusions

The 2020 and 2021 Antarctic ozone holes were among the largest on record despite the overall trend toward ozone recovery (<https://ozonewatch.gsfc.nasa.gov>; Stone et al., 2021). The results shown here reveal that both events were associated with changes in Southern Hemisphere surface climate consistent with the linkages between stratospheric ozone depletion and the large-scale SH circulation.

The results thus attest to the continuing role of stratospheric ozone depletion in surface climate change despite the onset of ozone recovery. They also indicate potentially important linkages between enhanced stratospheric particulate matter, ozone depletion, and changes in the hemispheric scale circulation from the stratosphere to the surface.

As discussed in the Introduction, the linkages between explosive volcanic eruptions and stratospheric ozone depletion are well established, whereas the linkages between wildfires and ozone depletion have only recently drawn comparable attention. Various mechanisms have been proposed. For examples: Yu et al. (2021) indicate significant simulated decreases in polar ozone following the 2020 Australian fires due to a combination of dynamical and chemical mechanisms. Solomon et al. (2022) show evidence for mid-latitude chemistry driving large observed nitrogen oxide changes following the fires. Santee et al. (2022) and Bernath et al. (2022) show remarkable changes in hydrochloric acid and chlorine nitrate at mid-latitudes after the Australian fires, but the chemical mechanism causing those changes has not yet been identified, nor has a clear link to polar chemistry been established. Wildfire soot may also contribute to dynamical changes in the strength of the vortex through changes in radiative heating, but this mechanism has yet to be explored.

The number of high aerosol loading events in the OMPS-LP record is limited and thus internal variability cannot be completely ruled out. Nevertheless, the results shown here are strongly suggestive of causal linkages between stratospheric aerosol loadings and widespread changes in Southern Hemisphere surface climate. Notably, the results highlight the intriguing possibility that catastrophic wildfires may have a profound effect on the hemispheric-scale circulation long after the cessation of smoke production.

Conflict of Interest

The authors declare no conflicts of interest relevant to this study.

Data Availability Statement

Data sets used in the analysis are freely available from the listed sources: OMPS-LP aerosol and ozone data are available at the Goddard Disc (https://disc.gsfc.nasa.gov/datasets/OMPS_NPP_LP_L2_AER_DAILY_2/summary?keywords=OMPS_NPP_LP_L2_AER_DAILY_2 and [https://disc.gsfc.nasa.gov/datasets/OMPS_NPP_LP_L2_O3_DAILY_2](https://disc.gsfc.nasa.gov/datasets/OMPS_NPP_LP_L2_O3_DAILY_2/summary?keywords=OMPS_NPP_LP_L2_O3_DAILY_2)), polar cap ozone data are

available from the website (<http://ozonewatch.gsfc.nasa.gov>), and ERA5 data are available at the Copernicus Climate Change Service Climate Data Store (<https://doi.org/10.24381/cds.bd0915c6>).

Acknowledgments

D. W. J. Thompson and S. Yook are supported by the NSF Climate and Large-Scale Dynamics program (AGS-1848785). S. Solomon is supported by NSF Climate and Large-Scale Dynamics program (AGS-1848863). We thank William Randel for comments on the results. S. Yook, D. W. J. Thompson, and S. Solomon designed the research and wrote the paper. S. Yook analyzed the data and produced the figures.

References

Abrahamsen, E. P., Barreira, S., Bitz, C. M., Butler, A., Clem, K. R., Colwell, S., et al. (2020). Antarctica and the Southern Ocean. *Bulletin of the American Meteorological Society*, 101(8), S287–S320. Retrieved from <https://journals.ametsoc.org/view/journals/bams/101/8/bamsD200090.xml>

Ansmann, A., Ohneiser, K., Chudnovsky, A., Knopf, D. A., Eloranta, E. W., Villanueva, D., et al. (2022). Ozone depletion in the Arctic and Antarctic stratosphere induced by wildfire smoke. *Atmospheric Chemistry and Physics Discussions*, 2022, 1–42. Retrieved from <https://acp.copernicus.org/preprints/acp-2022-247/>

Ansmann, A., Ohneiser, K., Mamouri, R.-E., Knopf, D. A., Veselovskii, I., Baars, H., et al. (2021). Tropospheric and stratospheric wildfire smoke profiling with lidar: Mass, surface area, CCN, and INP retrieval. *Atmospheric Chemistry and Physics*, 21(12), 9779–9807. <https://doi.org/10.5194/acp-21-9779-2021>

Babu, S. R., Nguyen, L. S. P., Sheu, G.-R., Griffith, S. M., Pani, S. K., Huang, H.-Y., & Lin, N.-H. (2021). *Long-range transport of La Soufrière volcanic plume to the western North Pacific: Influence on atmospheric mercury and aerosol properties*. *Atmospheric Environment*, 118806.

Baldwin, M. P., & Dunkerton, T. J. (2001). Stratospheric harbingers of anomalous weather regimes. *Science*, 294(5542), 581–584. <https://doi.org/10.1126/science.1063315>

Banerjee, D. S., Stephenson, G., & Das, S. G. (2020). *Segmentation and analysis of mother machine data: SAM*. bioRxiv.

Bernath, P., Boone, C., & Crouse, J. (2022). Wildfire smoke destroys stratospheric ozone. *Science*, 375(6586), 1292–1295. <https://doi.org/10.1126/science.abm5611>

Chen, Z., DeLand, M., & Bhartia, P. K. (2016). A new algorithm for detecting cloud height using OMPS/LP measurements. *Atmospheric Measurement Techniques*, 9(3), 1239–1246. Retrieved from <https://amt.copernicus.org/articles/9/1239/2016/>

Coupe, J., & Robock, A. (2021). The influence of stratospheric soot and sulfate aerosols on the Northern Hemisphere wintertime atmospheric circulation. *Journal of Geophysical Research: Atmospheres*, 126(11), e2020JD034513. <https://doi.org/10.1029/2020JD034513>

DallaSanta, K., Gerber, E. P., & Toohey, M. (2019). The circulation response to volcanic eruptions: The key roles of stratospheric warming and eddy interactions. *Journal of Climate*, 32(4), 1101–1120. <https://doi.org/10.1175/jcli-d-18-0099.1>

Fogt, R. L., & Marshall, G. J. (2020). The Southern annular mode: Variability, trends, and climate impacts across the Southern Hemisphere. *Wiley Interdisciplinary Reviews: Climate Change*, 11(4), e652. <https://doi.org/10.1002/wcc.652>

Hassler, B., Daniel, J., Johnson, B., Solomon, S., & Oltmans, S. (2011). An assessment of changing ozone loss rates at South Pole: Twenty-five years of ozonesonde measurements. *Journal of Geophysical Research*, 116(D22). <https://doi.org/10.1029/2011jd016353>

Hendon, H. H., Thompson, D. W., & Wheeler, M. C. (2007). Australian rainfall and surface temperature variations associated with the Southern Hemisphere annular mode. *Journal of Climate*, 20(11), 2452–2467. <https://doi.org/10.1175/jcli4134.1>

Hersbach, H., Bell, B., Berrisford, P., Hirahara, S., Horányi, A., Muñoz-Sabater, J., et al. (2020). The ERA5 global reanalysis. *Quarterly Journal of the Royal Meteorological Society*, 146(730), 1999–2049. <https://doi.org/10.1002/qj.3803>

Hirsch, E., & Koren, I. (2021). Record-breaking aerosol levels explained by smoke injection into the stratosphere. *Science*, 371(6535), 1269–1274. <https://doi.org/10.1126/science.abe1415>

Khaykin, S., Legras, B., Bucci, S., Sellitto, P., Isaksen, L., Tencé, F., et al. (2020). The 2019/20 Australian wildfires generated a persistent smoke-charged vortex rising up to 35 km altitude. *Communications Earth & Environment*, 1(1), 22. <https://doi.org/10.1038/s43247-020-00022-5>

Kidston, J., Scaife, A. A., Hardiman, S. C., Mitchell, D. M., Butchart, N., Baldwin, M. P., & Gray, L. J. (2015). Stratospheric influence on tropospheric jet streams, storm tracks and surface weather. *Nature Geoscience*, 8(6), 433–440. <https://doi.org/10.1038/ngeo2424>

Kodera, K. (1994). Influence of volcanic eruptions on the troposphere through stratospheric dynamical processes in the Northern Hemisphere winter. *Journal of Geophysical Research*, 99(D1), 1273–1282. <https://doi.org/10.1029/93jd02731>

Kramarova, N., Nash, E., Newman, P., Bhartia, P., McPeters, R., Rault, D., et al. (2014). Measuring the Antarctic ozone hole with the new Ozone Mapping and Profiler Suite (OMPS). *Atmospheric Chemistry and Physics*, 14(5), 2353–2361. <https://doi.org/10.5194/acp-14-2353-2014>

Langematz, U., Tully, M., Calvo, N., Dameris, M., de Laat, J., Klekociuk, A. R., et al. (2018). Polar stratospheric ozone: Past, present, and future, chapter 4 in WMO scientific assessment of ozone depletion (2018). *UNEP/WMO Scientific Assessment of Ozone Depletion: 2018 (Report)*, 58.

Magaritz-Ronen, L., & Raveh-Rubin, S. (2021). Wildfire smoke highlights troposphere to stratosphere pathway. *Geophysical Research Letters*, e2021GL095848. <https://doi.org/10.1029/2021GL095848>

Ohneiser, K., Ansmann, A., Baars, H., Seifert, P., Barja, B., Jimenez, C., et al. (2020). Smoke of extreme Australian bushfires observed in the stratosphere over Punta Arenas, Chile, in January 2020: Optical thickness, lidar ratios, and depolarization ratios at 355 and 532 nm. *Atmospheric Chemistry and Physics*, 20(13), 8003–8015. <https://doi.org/10.5194/acp-20-8003-2020>

Peterson, D. A., Fromm, M. D., McRae, R. H., Campbell, J. R., Hyer, E. J., Taha, G., et al. (2021). Australia's Black Summer pyrocumulonimbus super outbreak reveals potential for increasingly extreme stratospheric smoke events. *npj climate and atmospheric science*, 4(1), 1–16. <https://doi.org/10.1038/s41612-021-00192-9>

Polvani, L. M., Waugh, D. W., Correa, G. J., & Son, S.-W. (2011). Stratospheric ozone depletion: The main driver of twentieth-century atmospheric circulation changes in the Southern Hemisphere. *Journal of Climate*, 24(3), 795–812. <https://doi.org/10.1175/2010jcli3772.1>

Portmann, R., Solomon, S., Garcia, R., Thomason, L., Poole, L., & McCormick, M. (1996). Role of aerosol variations in anthropogenic ozone depletion in the polar regions. *Journal of Geophysical Research*, 101(D17), 22991–23006. <https://doi.org/10.1029/96jd02608>

Randel, W. J., & Wu, F. (1999). Cooling of the Arctic and Antarctic polar stratospheres due to ozone depletion. *Journal of Climate*, 12(5), 1467–1479. [https://doi.org/10.1175/1520-0442\(1999\)012<1467:cataaa>2.0.co;2](https://doi.org/10.1175/1520-0442(1999)012<1467:cataaa>2.0.co;2)

Randel, W. J., Wu, F., & Stolarski, R. (2002). Changes in column ozone correlated with the stratospheric EP flux. *Journal of the Meteorological Society of Japan. Ser. II*, 80(4B), 849–862. <https://doi.org/10.2151/jmsj.80.849>

Rieger, L., Randel, W., Bourassa, A., & Solomon, S. (2021). Stratospheric temperature and ozone anomalies associated with the 2020 Australian New Year Fires. *Geophysical Research Letters*, 48(24), e2021GL095898. <https://doi.org/10.1029/2021gl095898>

Robock, A. (2000). Volcanic eruptions and climate. *Reviews of Geophysics*, 38(2), 191–219. <https://doi.org/10.1029/1998rg000054>

Robock, A., & Mao, J. (1995). The volcanic signal in surface temperature observations. *Journal of Climate*, 8(5), 1086–1103. [https://doi.org/10.1175/1520-0442\(1995\)008<1086:vtis>2.0.co;2](https://doi.org/10.1175/1520-0442(1995)008<1086:vtis>2.0.co;2)

Safieddine, S., Bouillon, M., Paracho, A. C., Jumelet, J., Tence, F., Pazmino, A., et al. (2020). Antarctic ozone enhancement during the 2019 sudden stratospheric warming event. *Geophysical Research Letters*, 47(14), e2020GL087810. <https://doi.org/10.1029/2020gl087810>

Santee, M., Lambert, A., Manney, G., Livesey, N., Froidevaux, L., Neu, J., et al. (2022). Prolonged and pervasive perturbations in the composition of the southern Hemisphere midlatitude lower stratosphere from the Australian new year's fires. *Geophysical Research Letters*, 49(4), e2021GL096270. <https://doi.org/10.1029/2021gl096270>

Schwartz, M. J., Santee, M. L., Pumphrey, H. C., Manney, G. L., Lambert, A., Livesey, N. J., et al. (2020). Australian new year's pyroCb impact on stratospheric composition. *Geophysical Research Letters*, 47(24), e2020GL090831. <https://doi.org/10.1029/2020gl090831>

Shen, X., Wang, L., & Osprey, S. (2020). Tropospheric forcing of the 2019 Antarctic sudden stratospheric warming. *Geophysical Research Letters*, 47(20), e2020GL089343. <https://doi.org/10.1029/2020gl089343>

Shindell, D. T., & Schmidt, G. A. (2004). Southern Hemisphere climate response to ozone changes and greenhouse gas increases. *Geophysical Research Letters*, 31(18), L18209. <https://doi.org/10.1029/2004gl020724>

Shindell, D. T., Wong, S., & Rind, D. (1997). Interannual variability of the Antarctic ozone hole in a GCM. Part I: The influence of tropospheric wave variability. *Journal of the Atmospheric Sciences*, 54(18), 2308–2319. [https://doi.org/10.1175/1520-0469\(1997\)054<2308:ivota>2.0.co;2](https://doi.org/10.1175/1520-0469(1997)054<2308:ivota>2.0.co;2)

Solomon, S. (1999). Stratospheric ozone depletion: A review of concepts and history. *Reviews of Geophysics*, 37(3), 275–316. <https://doi.org/10.1029/1999rg00008>

Solomon, S., Dube, K., Stone, K., Yu, P., Kinnison, D., Toon, O. B., et al. (2022). On the stratospheric chemistry of midlatitude wildfire smoke. *Proceedings of the National Academy of Sciences*, 119(10), e2117325119. <https://doi.org/10.1073/pnas.2117325119>

Solomon, S., Ivy, D. J., Kinnison, D., Mills, M. J., Neely, R. R., & Schmidt, A. (2016). Emergence of healing in the Antarctic ozone layer. *Science*, 353(6296), 269–274. <https://doi.org/10.1126/science.aae0061>

Stone, K., Solomon, S., Kinnison, D., & Mills, M. J. (2021). On recent large Antarctic ozone holes and ozone recovery metrics. *Geophysical Research Letters*, 48(22), e2021GL095232. <https://doi.org/10.1029/2021GL095232>

Strahan, S. E., Douglass, A. R., & Damon, M. R. (2019). Why do Antarctic ozone recovery trends vary? *Journal of Geophysical Research: Atmospheres*, 124(15), 8837–8850. <https://doi.org/10.1029/2019jd030996>

Tabazadeh, A., Drdla, K., Schoeberl, M., Hamill, P., & Toon, O. (2002). Arctic "ozone hole" in a cold volcanic stratosphere. *Proceedings of the National Academy of Sciences*, 99(5), 2609–2612. <https://doi.org/10.1073/pnas.052518199>

Taha, G., Loughman, R., Zhu, T., Thomason, L., Kar, J., Rieger, L., & Bourassa, A. (2021). OMPS LP Version 2.0 multi-wavelength aerosol extinction coefficient retrieval algorithm. *Atmospheric Measurement Techniques*, 14(2), 1015–1036. <https://doi.org/10.5194/amt-14-1015-2021>

Thompson, D. W., Baldwin, M. P., & Solomon, S. (2005). Stratosphere–troposphere coupling in the southern Hemisphere. *Journal of the Atmospheric Sciences*, 62(3), 708–715. <https://doi.org/10.1175/jas-3321.1>

Thompson, D. W., & Solomon, S. (2002). Interpretation of recent Southern Hemisphere climate change. *Science*, 296(5569), 895–899. <https://doi.org/10.1126/science.1069270>

Thompson, D. W., Solomon, S., Kushner, P. J., England, M. H., Grise, K. M., & Karoly, D. J. (2011). Signatures of the Antarctic ozone hole in Southern Hemisphere surface climate change. *Nature Geoscience*, 4(11), 741–749. <https://doi.org/10.1038/ngeo1296>

Toohey, M., Krüger, K., Bittner, M., Timmreck, C., & Schmidt, H. (2014). The impact of volcanic aerosol on the northern Hemisphere stratospheric polar vortex: Mechanisms and sensitivity to forcing structure. *Atmospheric Chemistry and Physics*, 14(23), 13063–13079. <https://doi.org/10.5194/acp-14-13063-2014>

Wargan, K., Weir, B., Manney, G. L., Cohn, S. E., & Livesey, N. J. (2020). The anomalous 2019 Antarctic ozone hole in the GEOS Constituent Data Assimilation System with MLS observations. *Journal of Geophysical Research: Atmospheres*, 125(18), e2020JD033335. <https://doi.org/10.1029/2020jd033335>

Waugh, D. W., Randel, W. J., Pawson, S., Newman, P. A., & Nash, E. R. (1999). Persistence of the lower stratospheric polar vortices. *Journal of Geophysical Research*, 104(D22), 27191–27201. <https://doi.org/10.1029/1999jd900795>

Weber, M., Dikty, S., Burrows, J. P., Gurney, H., Dameris, M., Kubin, A., et al. (2011). The Brewer-Dobson circulation and total ozone from seasonal to decadal time scales. *Atmospheric Chemistry and Physics*, 11(21), 11221–11235. <https://doi.org/10.5194/acp-11-11221-2011>

Wilka, C., Shah, K., Stone, K., Solomon, S., Kinnison, D., Mills, M., et al. (2018). On the role of heterogeneous chemistry in ozone depletion and recovery. *Geophysical Research Letters*, 45(15), 7835–7842. <https://doi.org/10.1029/2018gl078596>

Yu, P., Davis, S. M., Toon, O. B., Portmann, R. W., Bardeen, C. G., Barnes, J. E., et al. (2021). Persistent stratospheric warming due to 2019–2020 Australian wildfire smoke. *Geophysical Research Letters*, 48(7), e2021GL092609. <https://doi.org/10.1029/2021gl092609>

Zambri, B., Solomon, S., Thompson, D. W., & Fu, Q. (2021). Emergence of Southern Hemisphere stratospheric circulation changes in response to ozone recovery. *Nature Geoscience*, 14(9), 638–644. <https://doi.org/10.1038/s41561-021-00803-3>

Zawada, D. J., Rieger, L. A., Bourassa, A. E., & Degenstein, D. A. (2018). Tomographic retrievals of ozone with the OMPS Limb profiler: Algorithm description and preliminary results. *Atmospheric Measurement Techniques*, 11(4), 2375–2393. <https://doi.org/10.5194/amt-11-2375-2018>

Zhu, Y., Toon, O. B., Kinnison, D., Harvey, V. L., Mills, M. J., Bardeen, C. G., et al. (2018). Stratospheric aerosols, polar stratospheric clouds, and polar ozone depletion after the Mount Calbuco eruption in 2015. *Journal of Geophysical Research: Atmospheres*, 123(21), 12–308. <https://doi.org/10.1029/2018jd028974>